

BBXRT Calibration Update - test18

Kimberly Weaver

June 1, 1992

1 Quick Summary

The BBXRT response matrix has now been adjusted to a best estimate (effective area, partial charge) for all pixels and the latest on-axis versions are available in `/xanadu/spectral/bbxrt`. You can create your own matrix using `bbxrtrsp` and the probability matrices `quadproba0...b4`. The test18 effective area curve was generated by modifying the mirror effective area curve (Figure 1) using XSPEC to fit the Crab for various detector absorption parameters. A0, B0 and the outer A pixels (A1,A2,A3) are reliable down to their lowest useable energies, determined by the detector noise threshold set in the electronics. However, because of the large correction and uncertainty in modeling the partial charge, the outer B pixels are reliable only down to about 0.5-0.7 keV. Table 1 lists the lowest available channels and the lowest reliable channels for all pixels along with their corresponding energies.

Figures 2a and 2b show the test18 on-axis, total effective area curves for A0 and B0. A comparison of the total (normalized) test18 effective area to the test16 effective area for A0 is given in Figure 3a. An enlargement between .4-.9 keV is shown in Figure 3b. This illustrates the difference between including oxygen (test16) versus Au N edges (test18). An enlargement around the aluminum, silicon and gold M edges is shown in Figure 3c. The test18 response matrix includes more aluminum and less silicon than test16. Figure 3d illustrates the addition of a nickel edge (Energy=8.3 keV) to the matrix.

At the present time, no residuals exist over 10% in A0 or B0. Plots of the residuals to the Crab are shown in Figure 4 which illustrates the best fit for an on-axis Crab observation (580 cnts/sec in A0; time 3.0569-3.068) that was used to adjust the effective areas for test18. Figures 4a and 4b show the ratio of the data to the best fit powerlaw ($\Gamma = 2.1$, $N_H = 0.3 \times 10^{22}$) for A0 and B0. [For comparison, and to point out our progress, Figure 4c shows the same ratio for A0 to a fit with the

test16 matrix.] It can be seen that there are 10% residuals remaining at 0.41 keV. Fitting with a narrow gaussian ($E=0.41$ keV) gives an EQW < 140 eV in A0 and < 220 eV in B0. Also there are 10% negative narrow residuals at 0.52 keV (slightly lower energy than an oxygen edge - 0.53 keV). Fitting with a notch (width 0.03) gives a covering fraction of < 0.4 for A0 and < 0.65 for B0.

However, splitting the Crab data into two files (which happen to be night(3.057-3.062) and day (3.062-3.068)) there is an indication that these low energy residuals change with time (Figure 5). In A0, they are present in the day data but disappear in the night data (Figures 5a,5b). For B0, the residuals are absent in the background subtracted daytime data but present in the night data (Figures 5c,d). So far I have investigated the guard rate, LED rate, earth angle and background subtraction as a source of the appearance and disappearance of the residuals. I believe the problem may not be with the effective area calibration, but that the low energy gain/resolution has changed for some reason. An alternative explanation would be that a source of soft photons was partially in our field of view during this Crab observation. To better illustrate the observed residuals, Figure 6 shows the .3-3 keV ratio of the unbinned data to the model for all four sets of data.

Other residuals include a 5% narrow feature at 1.38 keV (EQW < 10 eV) in both A0 and B0 (see Figures 4a,4b). There are also 5% residuals around aluminum and silicon and just above the silicon edge. A small "bump" still exists ($< 5\%$) around 7.5 keV in both central pixels while the high energy tail in B0 has still not been completely removed (10% above 10keV - see Figure 4b).

Table 1: BBXRT lowest energy Effective Area reliability

detector	low pha channel	Energy (keV)	low reliable channel	Energy (keV)
A0	16	0.29	16	0.29
A1	26	0.41	26	0.41
A2	26	0.42	26	0.42
A3	27	0.44	27	0.44
A4	25	0.41	28	0.46
B0	17	0.30	17	0.30
B1	27	0.42	39	0.60
B2	28	0.43	34	0.52
B3	28	0.45	34	0.54
B4	29	0.44	45	0.69

2 Description of procedure for effective area modification

It was the idea of the calibration committee to make the effective area adjustments separable and easy to reproduce by allowing modification of the detector absorptions without fudging the mirror effective area. Keeping in line with this idea, the response generating program had already been split into two - one which contained the gain, resolution, partial charge (i.e. everything having to do with redistributing the energy of the incoming photon) which is called *bbxrtmat* and produces the probability matrices *quadprob...* The second program *bbxrtrsp* reads in the mirror effective area, modifies it (including vignetting, detector effects, etc) and then multiplies this with the probability matrix.

Initially, P. Serlemitsos generated a total mirror effective area curve (Figure 1) for a mirror gold density (ρ) of 0.87. This value had been arrived at by fitting the Crab with an early response matrix that did NOT include nickel, and adjusting ρ to give the "correct" Crab slope ($\Gamma = 2.09$). A model called *detabs* was included in XSPEC which allowed the fitting of various detector absorptions (parylene, O, Al, Si, Au, Ni). The specification values (supplied by Peter and listed in Table 2, line 1) were tried and did not give a very good fit to the Crab (Figure 7), so they were allowed to vary. However, fitting the on-axis Crab data when including nickel gave a slope that was too steep. Peter then created a file which is read by *bbxrtrsp* and multiplies the areas to effectively change the mirror gold density from 0.87 to 0.84 (Figure 8). This works to flatten the Crab slope to $\Gamma = 2.1$. The effect of varying ρ is illustrated in Figure 9.

The next step was to adjust the areas to reduce the high energy tail (see Figure 4c) which had not been removed by adding nickel (i.e. our effective area was still underpredicted at > 6 keV). The 2-10 keV Crab data was fit using a matrix including nickel ($\Gamma = 2.09$, $N_H = 0.3 \times 10^{22}$) and the ratio of the data to the model was extracted for A0 and B0 separately and fit in QDP with a linear curve. This resulted in two correction files which are read in by *bbxrtrsp* and multiply the effective area. This correction is illustrated in Figure 10. The result is a slope of 2.11 to the Crab (2-10 keV) with the high energy excess essentially removed for on-axis sources. In addition, although the nickel edge has been removed in A0 (Figure 11a), it is a larger effect in B0 (Figure 11b) and needs to be more accurately measured.

To improve the low energy effective area reliability, the first thing necessary to determine is whether a dust halo should be included in fitting the Crab. If we are seeing the effects of dust, then because of our spatial resolution and the extent of the Crab, when the source is centered in A0, we should see a lower column density in the outer pixels. This is because low energy photons are being scattered into a halo (i.e. the source is larger at softer energies) and we see correspondingly more soft photons in the outer pixels. Similarly, when the Crab is off-axis, we should see a lower N_H in A0 relative to the on-axis A0 column. Figure 12 shows the ratio of the data to the model in the latter case. We are seeing about the same column in A0 as when the source is centered. Also, a fit to the summed

outer A pixel data (when the Crab is centered) gives $N_H = 0.3 \times 10^{22}$ (Figure 13). In addition, when one includes the dust model in A0, the fit is not statistically improved if the column is allowed to vary because adding dust merely mimics adding N_H (i.e. the measured column decreases). Since there is no strong evidence for a difference between pixels due to the dust, it is left out for the sake of simplicity. However, Figure 13 shows that the Crab spectrum is not well described by a single powerlaw in the outer pixels when the source is on-axis.

The test16 effective areas did contain oxygen which was added to help match the Crab at low energies but was not really expected since we didn't have much oxygen in the detector. From ground calibration measurements it is observed that the anomolous low energy absorption on detector B is probably due to gold instead of ice. Also, keeping oxygen in the matrix left some odd residuals around 0.6 and 0.8 keV which were finally removed by adding edges at 0.546, 0.643, and 0.762 due to Au N edge features (which had not been included in test16).

The largest uncertainties still present in the low energy effective areas are in the outer B pixels which have a larger partial charge (defined as the low energy tail to the response to a monoenergetic photon - due to charge being lost in the dead layer of the detector). I have not tried to remove the < 0.6 keV excess seen in the Crab data in the outer B pixels (Figure 14) because to do it with our step function partial charge model requires too much step (for a complete description of the current partial charge model see section 5 in *Notes on Pre-launch Calibration - May 1990*, prepared by the Calibration team). It seems clear from the outer B pixel data that our model for the shape of the partial charge is not right and needs to be further investigated using NIST data.

In order to adjust the area of the outer B pixels, I included the highest value for the step partial charge which did not give too much p.c. for the airglow lines. I then adjusted the silicon and parylene to give the same fit to a given Calibration source as I obtained in the corresponding A pixel. The cross-calibration sources used were: the Crab, Cyg X-1, Cyg X-2, PKS2155, capella, airglow data, and Perseus (as a flat- field). For test18, I was able to obtain consistency between all pairs of pixels for each target in those respective pairs. I was also able to obtain consistency between the A0/B0 and outer pixels for all pairs of on/off-axis observations of all targets except Cyg X-2. I believe this is due to something fundamentally different about the source spectrum between two different observations.

3 Changes made between test16 and test18:

- (1) Only matrices with quadratic gain are available.
- (2) A nickel edge has been included with 0.1 covering of nickel and a 50,000 Angstrom column (specification value).

- (3) The step partial charge constant term has been reduced in pixels A0,A1,A2,A3 and increased in pixels A4,B0,B2,B3,B4. The values are listed in Table 2, column 2. The percentage change from the test16 partial charge value is given in column 3.
- (4) Detector absorption values have been modified to match as closely as possible the test16 effective area in A0 and the low energy absorption seen in the B detector (Table 2).

Table 2: Detector values (absorption units in Angstroms) are as follows:

detector	p. c.	p. c. change	Parylene C_8H_8	Aluminum	Silicon	Gold1	Gold2
spec			4000	1500	900	200	
A0	3.40E-05	-15%	8150	1625	-100	126	0.0
A1	3.40E-05	-40%	8150	1625	-100	126	0.0
A2	3.40E-05	-40%	8150	1625	-100	126	0.0
A3	3.40E-05	-40%	8150	1625	-100	126	0.0
A4	7.50E-05	+25%	8150	1625	-100	126	0.0
B0	4.40E-05	+10%	11000	1900	-1000	212	44944
B1	6.00E-05	0 %	4400	1900	-2650	212	44944
B2	9.00E-05	+50%	5500	1900	-2000	212	44944
B3	9.00E-05	+50%	11000	1900	-3200	212	44944
B4	7.00E-05	+15%	8250	1900	-3300	212	44944

Notice the A pixels are consistent, in that the *detabs* values are the same for all A pixels. The differences between A and B are mostly in the amount of silicon and gold wanted. B wanted partial covering gold described by:

$$abs = Gold1 \times z - Gold2 \times z^2$$

where *Gold1* is the number of clumps times thickness, *Gold2* is the number of clumps times thickness squared, and *z* is defined as the energy dependent absorption cross-section.

The amount of silicon included in the test16 matrix is claimed to be 900 angstroms for the detector as well as some contribution to the edge from the partial charge model. In addition, it is assumed that we know the amount of silicon to the Crab. Simply fitting the Crab using test16 and the *detabs* model immediately requires the removal of 600 Angstroms of silicon in A0, so there is obviously too much silicon in the test16 matrix. However, since we don't know what the cause of the apparent excess silicon is, the fact that the Crab appears to want negative silicon (test18) is physically meaningless and implies we don't understand one or more of the following: the effects of the partial charge around the silicon edge, the thickness of the silicon layer in the detector or the silicon column to the Crab. The value of the *detabs* silicon parameter simply serves as a variable which allows improvement of the fit to the Crab. This also affects the best fit parylene value causing it to be too high due to the fact that it is compensating for the silicon at low energies.

- (5) Normalization correction - The default area in test16 was the area for two central pixels corrected for the point spread function. Now the effective area is for one telescope only.
- (6) To remove low energy residuals in the Crab and Cyg X-2, edges corresponding to Au N at energies 0.546, 0.643, and 0.762 keV have been added to the matrix. This eliminates the need for mysterious excess oxygen on the detector. The absorption depths of the edges are as follows: 0.3, 0.18, and 0.12 respectively for A with 0.66, 0.12, and 0.16 for the B detector.
- (8) The gold M edge (2.2keV) has been moved up two channels (32 eV) in the B mirror effective area curve to match the data. This is a little more than one would expect, but it is not unreasonable that the B edge energy would differ from that seen in A. In fact, experiments to study x-ray absorption fine structure allow the main edge energy to be a free parameter (Lee et al. 1981). There is an intrinsic uncertainty in determining the threshold energy of the edge due to variations in the density of states near the Fermi energy causing structure within ± 10 eV of E_o . Also chemical bonding effects can shift the apparent edge towards higher energies by up to 15 eV (Agarwal 1991, Lee et al. 1981).
- (9) The high energy excess of photons in the Crab has been corrected by multiplying the mirror effective areas by a relation of the form $R = m \times E + b$ above 0.52 keV (Figure 9), where m is 0.0429 and 0.055 for A and B respectively, and b is 0.772 and 0.708 for A and B. One possible reason for high energy flattening in the Crab spectrum is that we are seeing the contribution from the pulsar.
- (10) The slope for the Crab became too steep after adding nickel. This was corrected by multiplying the areas by a correction as a function of energy to change ρ from 0.87 to 0.84. In A0, the present fit to the Crab (2-10 keV) is $N_H = 0.3 \times 10^{22}$, $\Gamma = 2.1$. The file used to change the density is called *corrcoeffa0* and this was smoothed out around the Gold M edge.

4 remaining systematic problems:

- The nickel edge has not been measured (will be done at NIST), only the nominal values are included at the present time (F. Marshall). More accurate measurements should improve the B pixel which has a larger edge.
- There is an indication that the low energy detector gain/resolution may change with time and/or count rate (see Figure 5). This is presently under investigation.
- There is some disagreement in the literature on the "correct" or measured value of N_H to the Crab. With the Einstein SSS, the N_H was assumed to be 0.35×10^{22} without including dust scattering (Nick White, private comm). The Wisconsin rocket flight measured a value of 0.27

(Burrows 1982), while the FPCS measured an N_H of 0.35×10^{22} including a scattering halo (Schattenberg and Canizares, 1986). We have been fitting a value of $0.3 - 0.31$ for the Crab (without dust) going back to version test10 of the response. The dust halo is not required by our data, but if it is included at measured ROSAT values, the observed N_H decreases to 0.27×10^{22} .

- There are positive residuals in the Crab data at 1.38 keV. This appears to be a problem associated with a non-understanding of the matrix rather than a possible feature in the Crab. This is at worst a 10% residual (less than 10 eV EQW). See Figure 4a,b.
- The issue of the shape of the low energy tail to the response to a monoenergetic photon (the partial charge), as well as the effects around the silicon edge have been dropped for now pending analysis of new calibration data from NIST. A full understanding of the partial charge is needed to utilize the low energy outer B pixel data.
- The slope of off-axis sources seems to be too steep with our vignetting corrections. This may in part be due to the fact that the vignetting has been calculated using $\rho=0.87$ (the mirror density in test16) instead of 0.84 (test18 density).
- The significance of the high energy tail and the residuals around the Gold edge become worse as the source moves off-axis. This is illustrated in Figure 14 using a 4 arcminute off-axis observation of the Crab in pixel B3. Indications are that we are not correctly predicting the vignetting corrections. However, we may never be able to fully account for this since we don't have enough high-count rate sources to model the behavior as a function of off-axis angle.
- The gain is still off by about a channel in B3 and B4 at 0.5 keV.
- There remains an overall broad shape to the low level residuals to the Crab - decreasing from 2-4 keV and then increasing again. This is best illustrated in Figures 4a and 4b.

5 References

Agarwal, B.K. 1991, *X-Ray Spectroscopy* 2nd edition (New York: Springer-Verlag), pp. 252-254.

Burrows, D. 1982, Ph.D. thesis.

Lee, P.A., Citrin, P.H., Eisenberger, P. and Kincaid, B.M. 1981, *Reviews of Modern Physics*, Vol. 53, No. 4, p. 769.

Schattenburg, M.E. and Canizares, C.R. 1986, *Ap. J.*, 301, 759.

6 Figure Captions

Figure 1. Total BBXRT Mirror effective area curve (supplied by Peter Serlemitsos).

Figure 2. Total on-axis mirror + detector effective area curve. a) For pixel A0. b) For pixel B0.

Figure 3. Comparison of test18 effective area to test16 effective area for channels 17-512. Test18 (solid line) is re-normalized to the test16 area (i.e. area for two telescopes). a) Total effective area. b) Enlargement around gold N edges to illustrate the difference between having gold and oxygen in the matrix. c) Enlargement around aluminum, silicon and gold M edges. d) Enlargement around the nickel edge.

Figure 4. Ratio of the data to a power law model fit to the Crab on-axis data using test18. This data file contains both daytime and nighttime data. a) For Pixel A0. b) Pixel B0 - notice the high energy tail has not been completely removed. c) Fit to the same data using test16.

Figure 5. Plots of data and model plus residuals to the on-axis Crab data using test18. The model parameters are best fit values. a) A0 pixel, night data ($N_H = 0.304 \times 10^{22}$, $\Gamma = 2.1$). b) A0 pixel, day data ($N_H = 0.306 \times 10^{22}$, $\Gamma = 2.1$). c) B0 pixel, night data ($N_H = 0.31 \times 10^{22}$, $\Gamma = 2.1$). d) B0 pixel, day data ($N_H = 0.308 \times 10^{22}$, $\Gamma = 2.1$).

Figure 6. Ratio of the 0.3-3 keV Crab data to the model for fits in Figure 5. The data are unbinned.

Figure 7. Powerlaw fit to the Crab using the Mirror effective area and the specification detector absorption values (Table 1, line 1). This was an attempt to use XSPEC to mimic the test16 response matrix.

Figure 8. Mirror density correction vs. energy applied to the areas to change the mirror gold density from 0.87 to 0.84. The curve was produced by dividing the mirror effective area curve generated having $\rho = 0.84$ by the effective area curve having $\rho = 0.87$.

Figure 9. Illustration of the effects of changing the Mirror gold density parameter on the mirror effective area curve. Generated using Rob Petre's ray tracing program.

Figure 10. High energy excess correction file which is a fit to the ratio of the > 5.2 keV data to the model for the Crab (2-10 keV) fit with a powerlaw. This multiplies the effective areas.

Figure 11. Present high energy residuals for the Crab fit to a powerlaw. a) pixel A0. b) pixel B0.

Figure 12. Ratio of the data to the model for the off-axis Crab observation in pixel A0, fit using the test18 response matrix.

Figure 13. Ratio of the data to the model for the summed A1,A2 and A3 data when Crab is on-axis. The fit is $N_H = 0.295 \times 10^{22}$, $\Gamma = 2.1$.

Figure 14. Ratio of the data to the model for a 4 arcminute off-axis Crab observation in pixel B3. The low energy and high energy residuals illustrate our remaining problems in outer pixels (due to partial charge) and for off-axis observations (due to incorrect vignetting?) respectively.

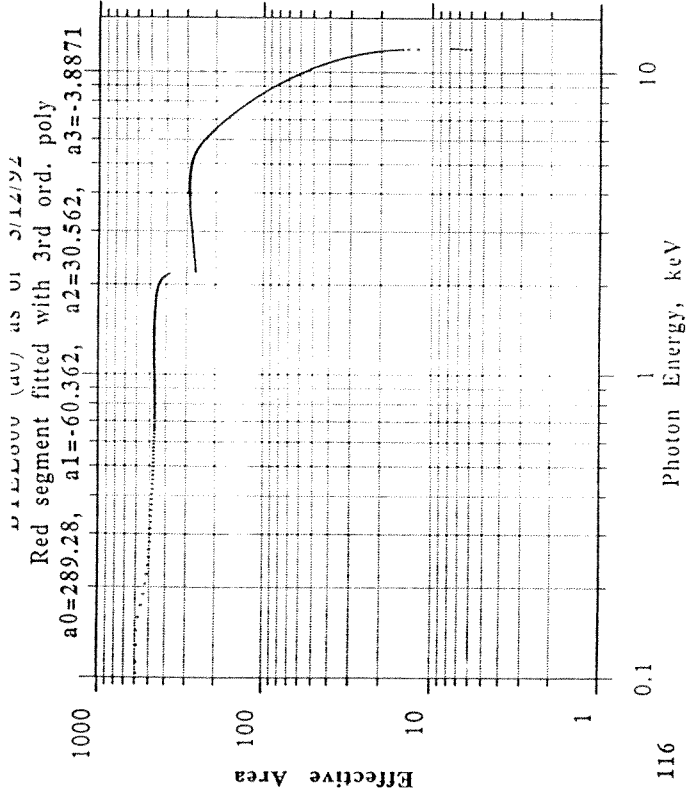


Fig. 1

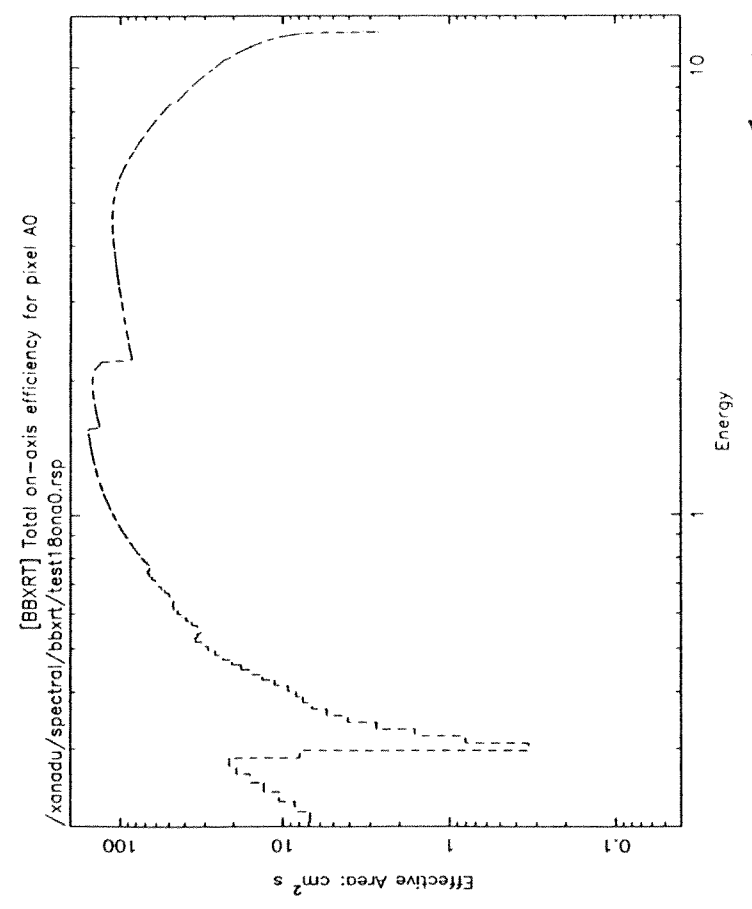


Fig. 2a

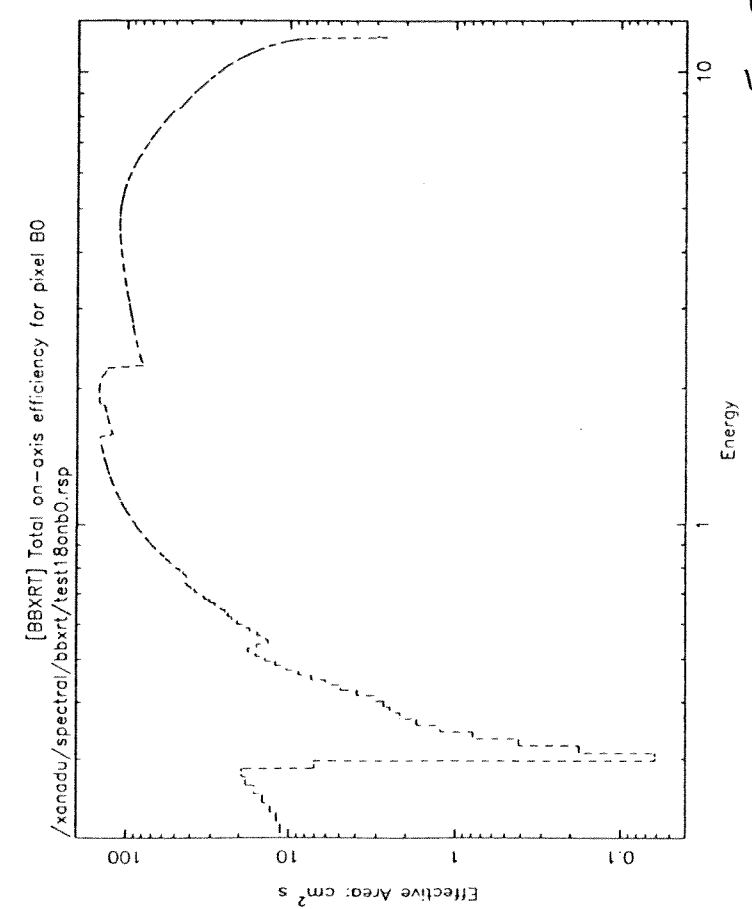


Fig. 2b

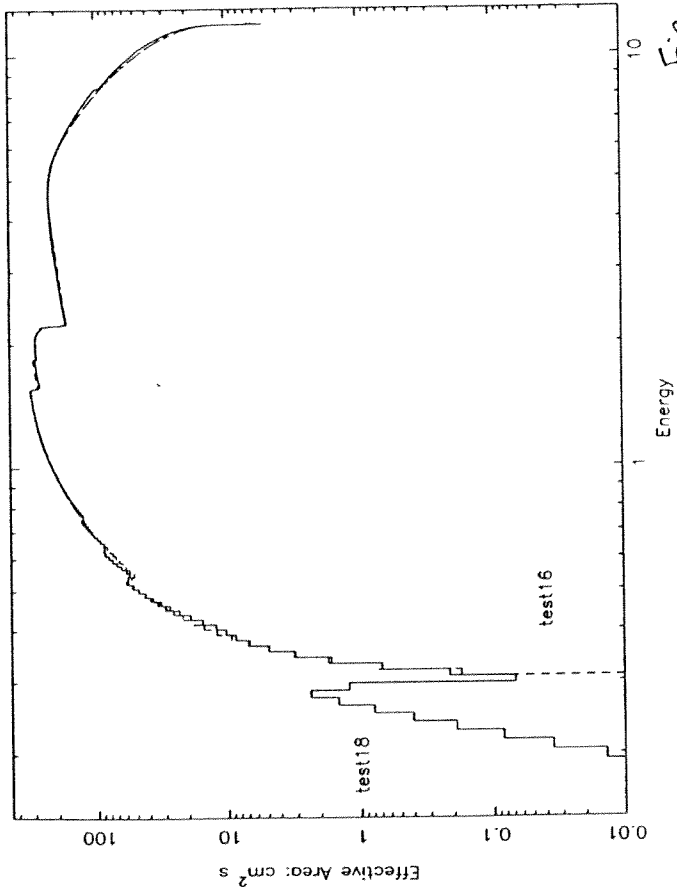


Fig. 3a

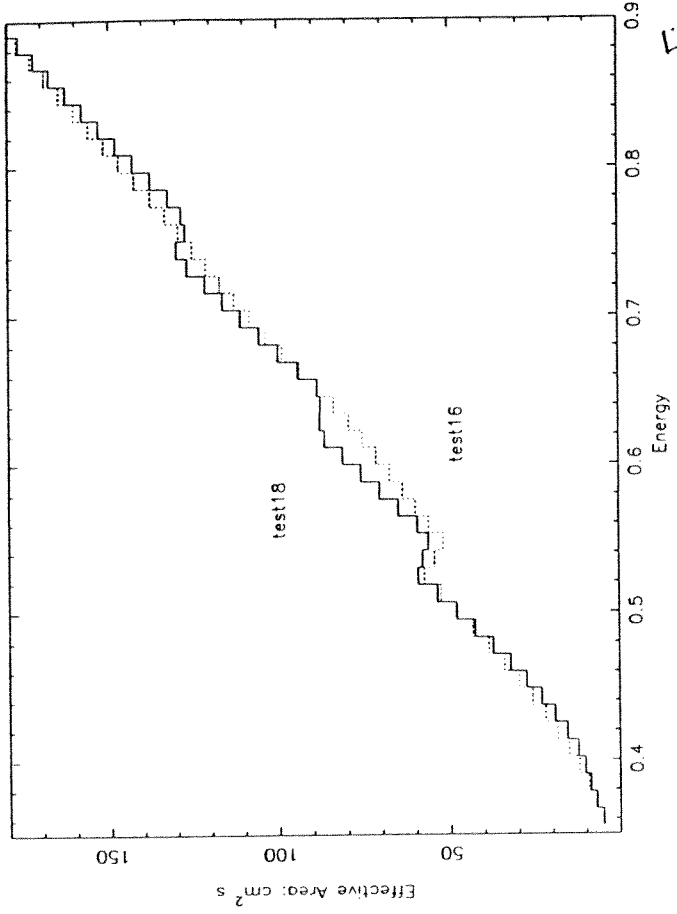


Fig. 3b

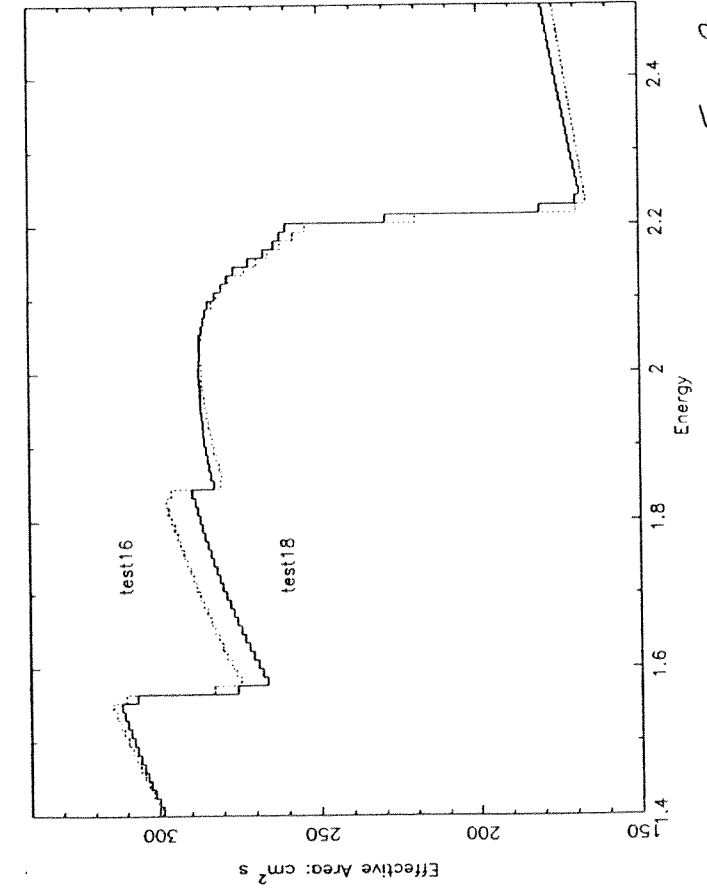


Fig. 3c

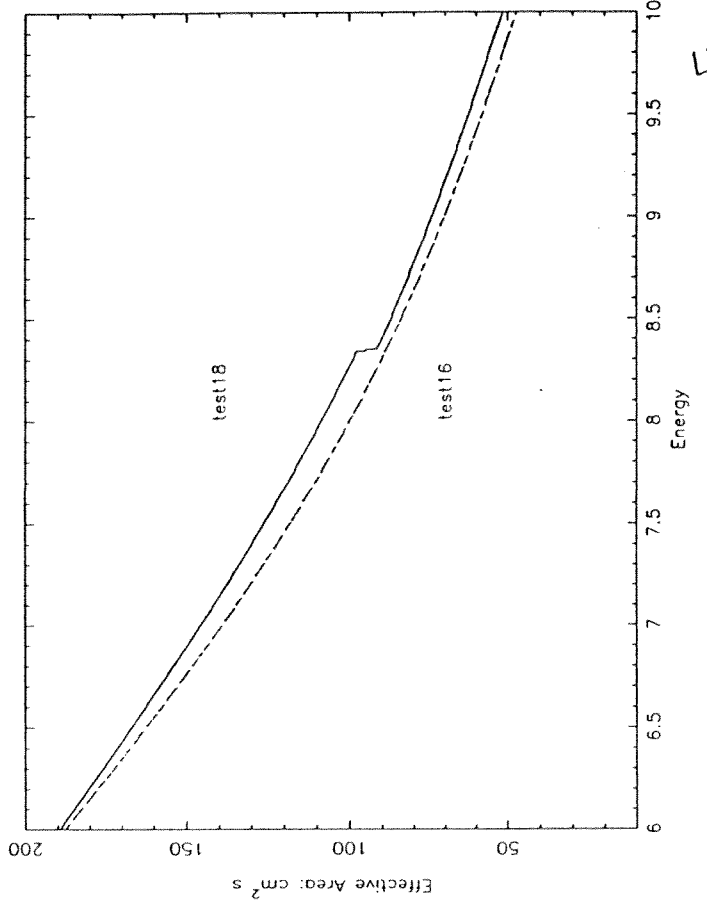


Fig. 3d

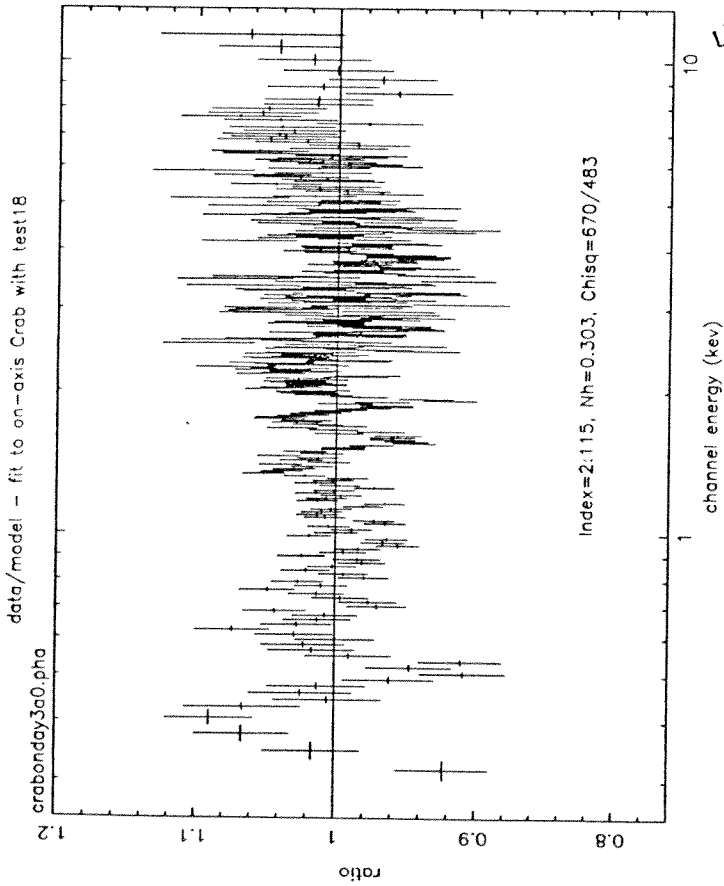


Fig. 4a

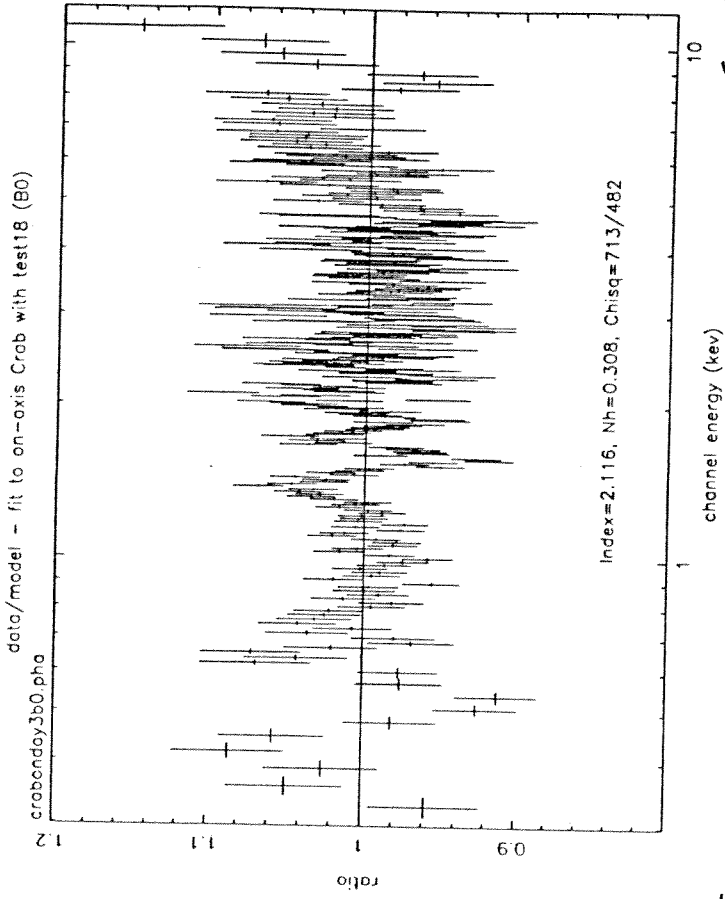


Fig. 4b

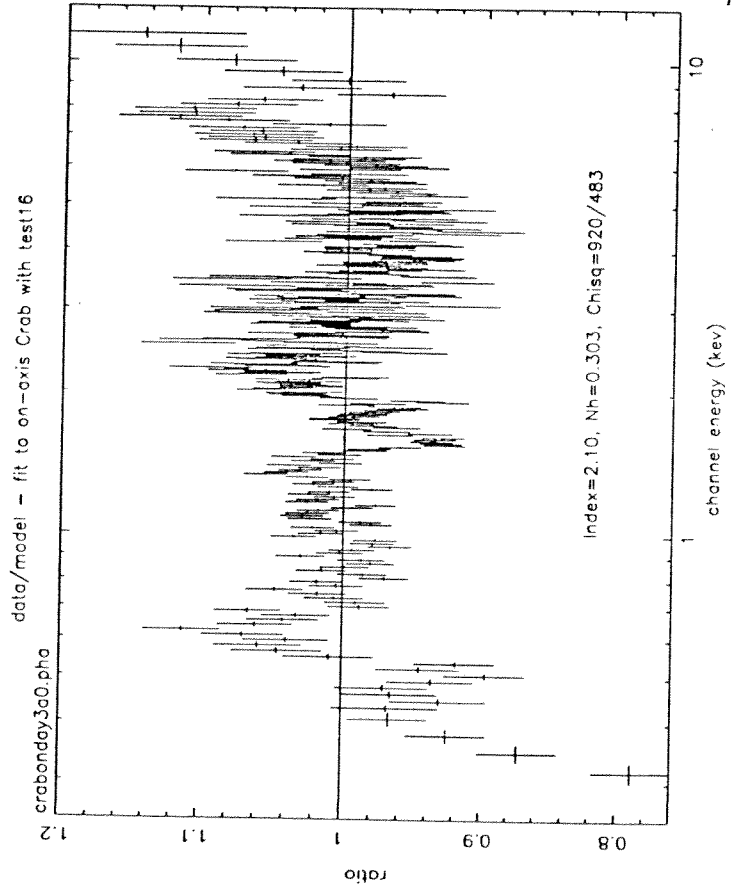


Fig. 4c

data and folded model AO Night w/ test18

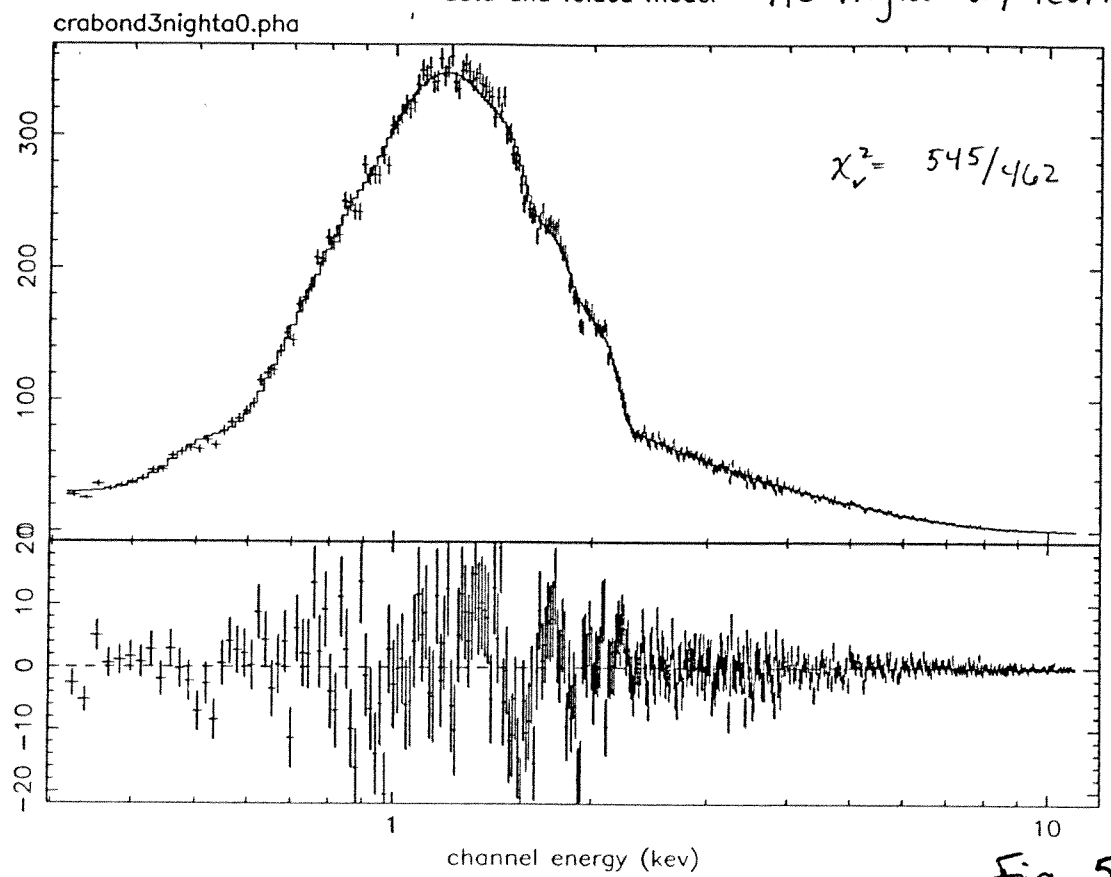


Fig. 5a

data and folded model AO Day w/ test18

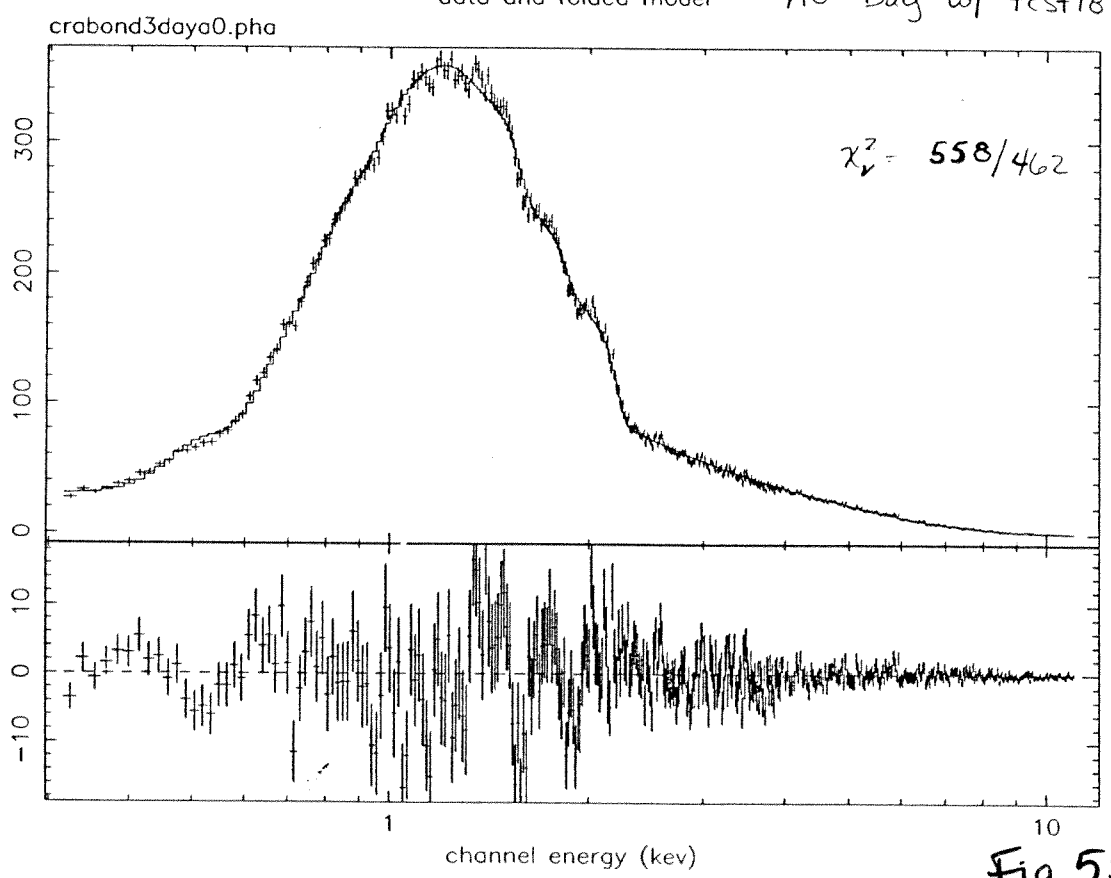


Fig 5b

data and folded model BO Night w/ test18

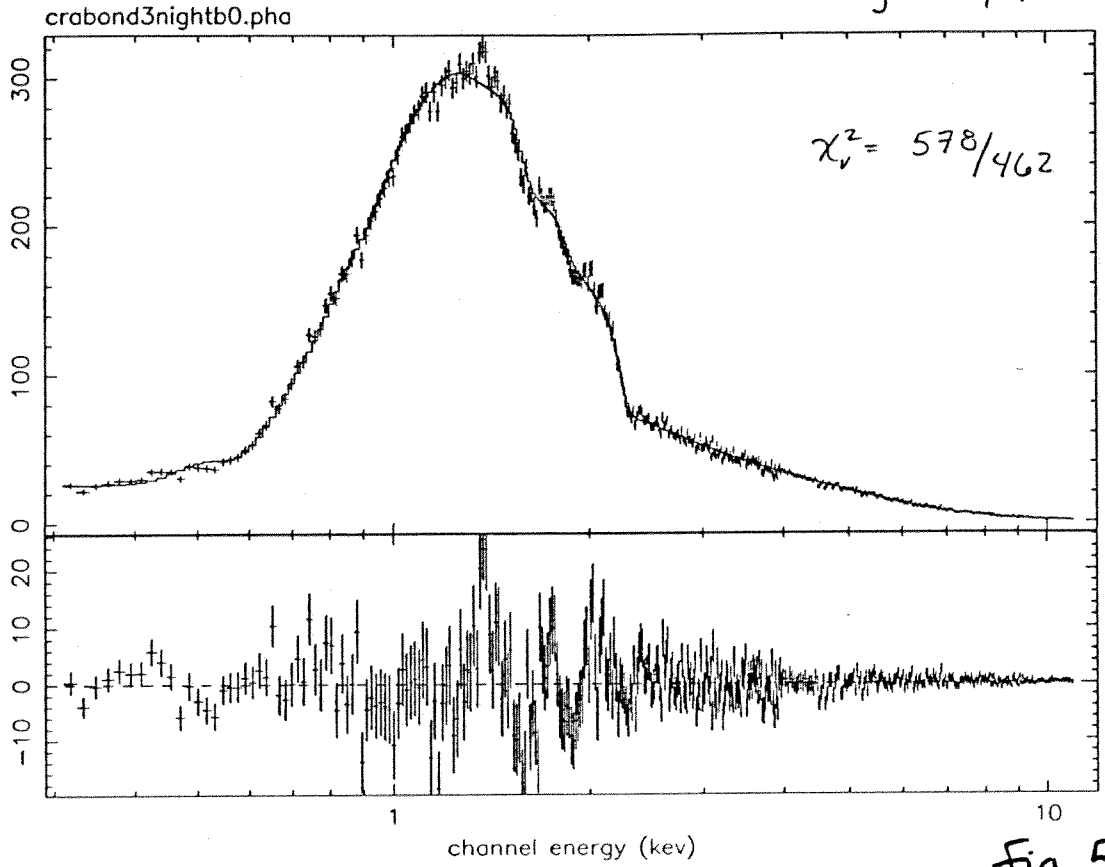


Fig. 5c

data and folded model BO Day w/ test18

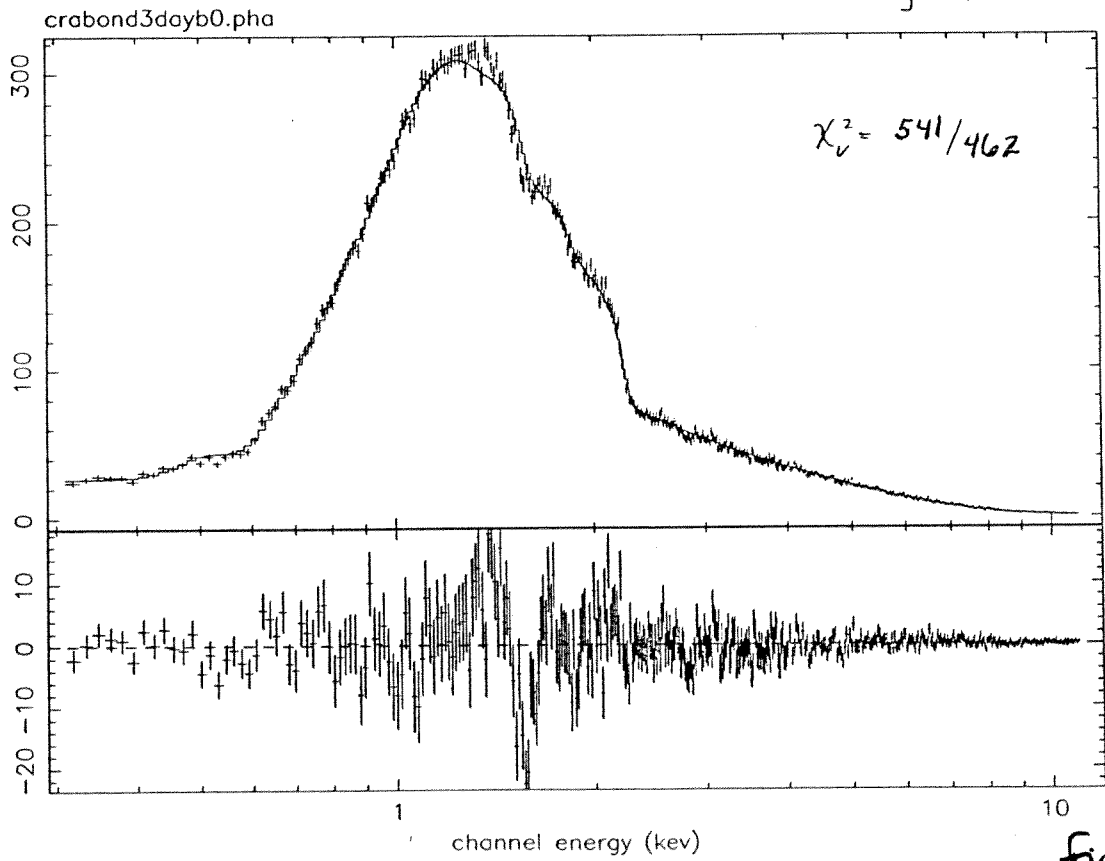
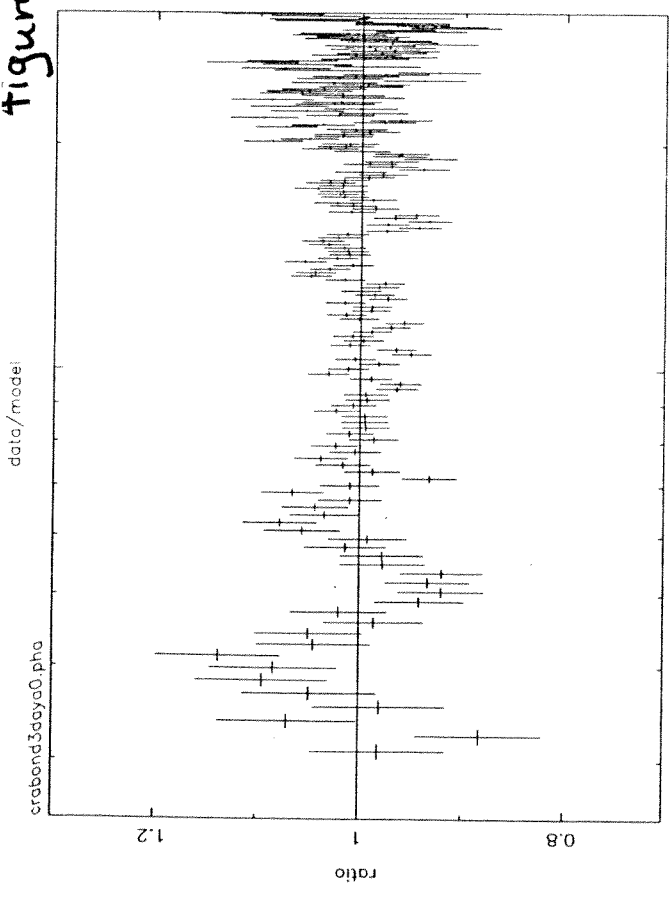
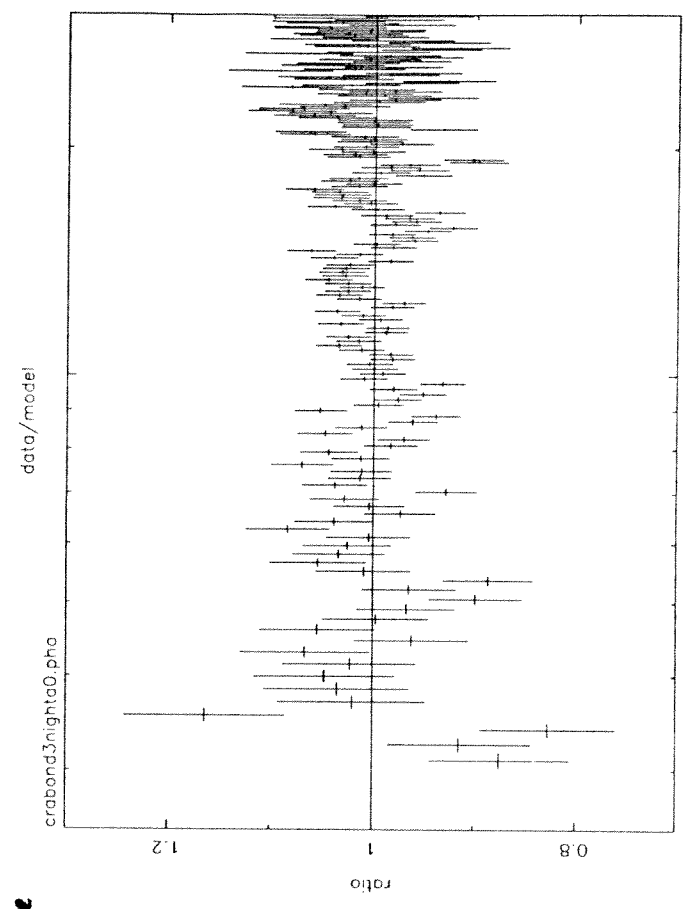


Fig. 5d

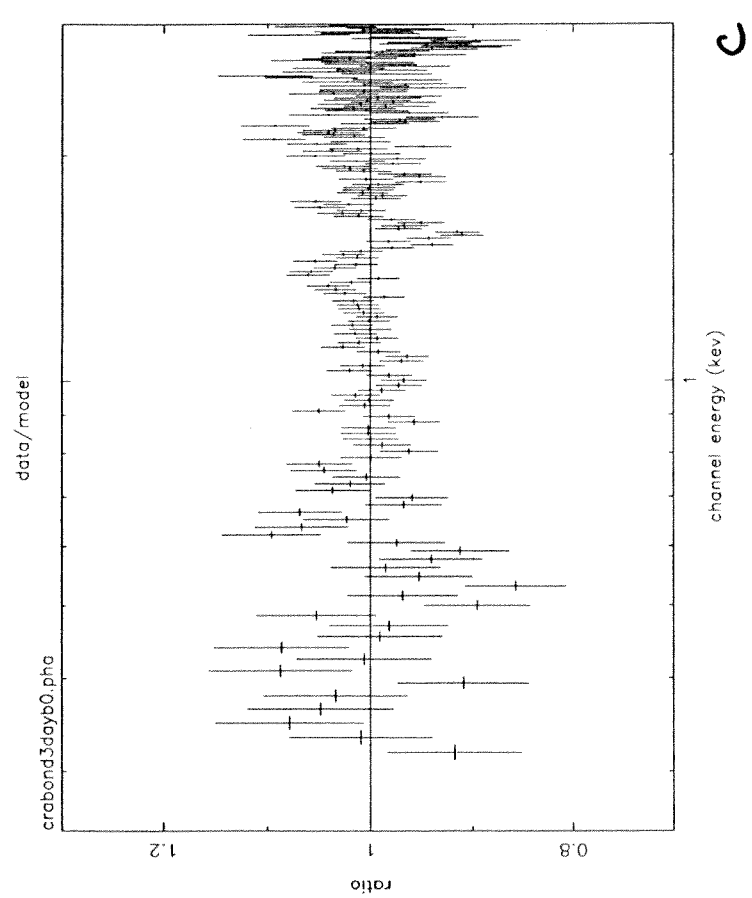
Figure 6



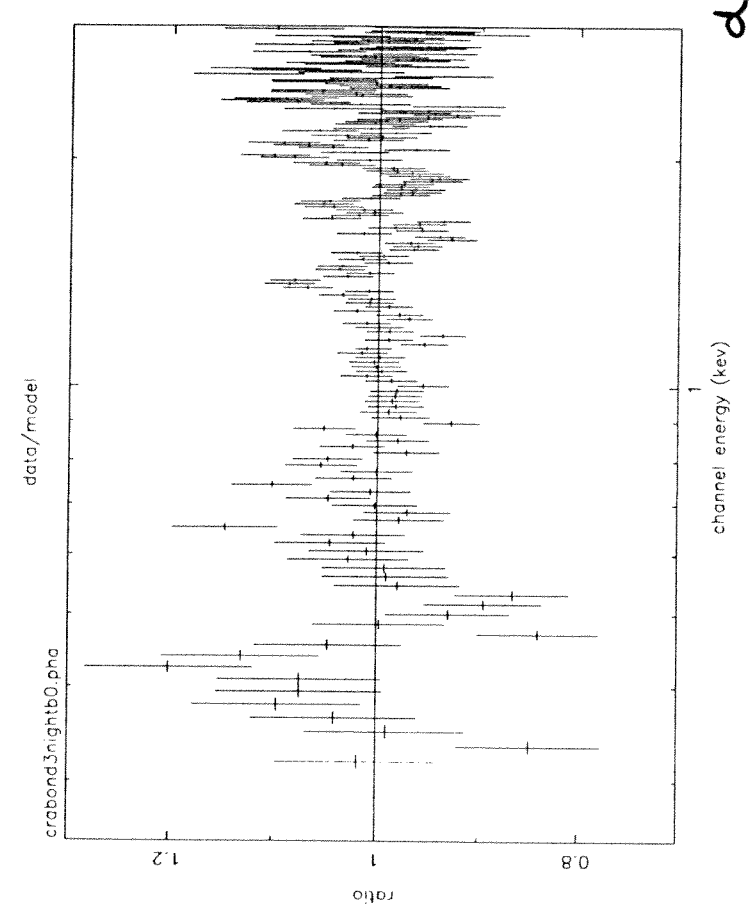
a



b



c



d

Crab fit w/ test16mirror0 using nominal values
crabonday3a0.pha

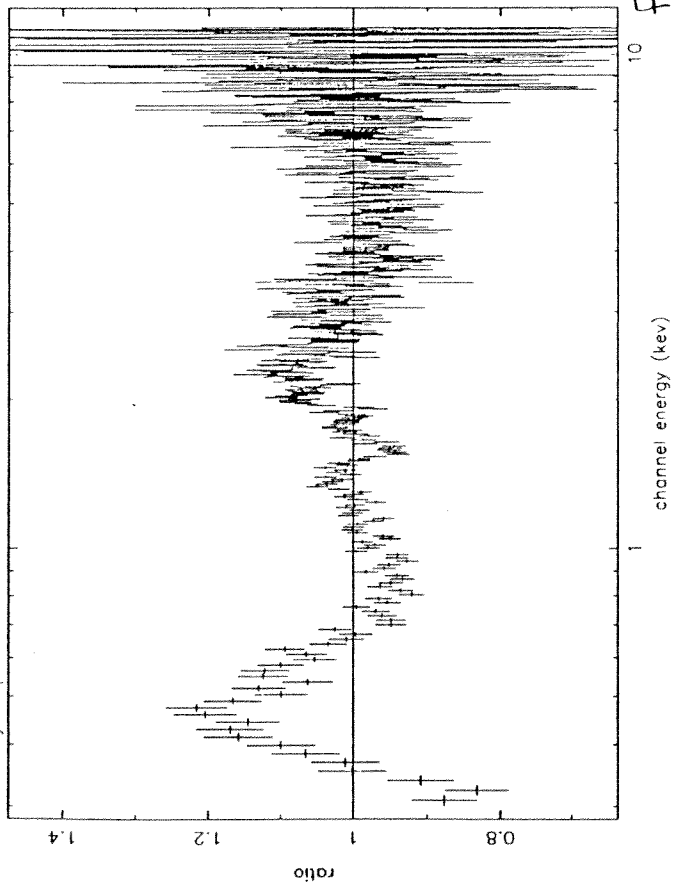


Fig. 7 127 4/10/92

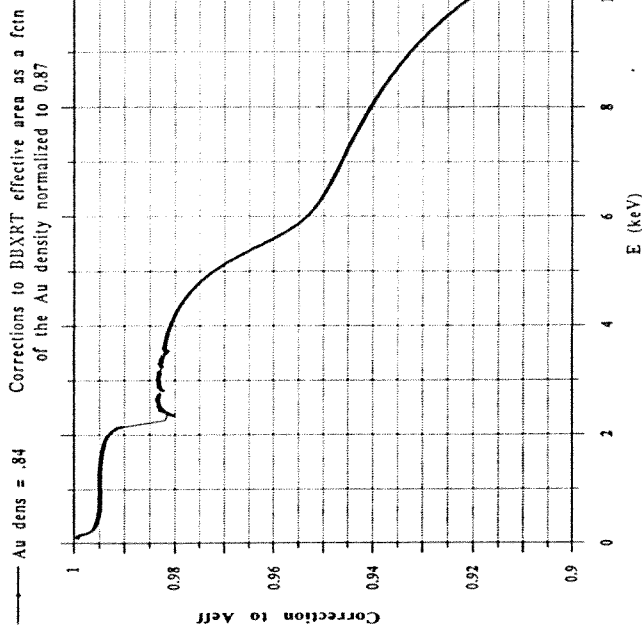


Fig. 8

Effects of varying gold density on effa

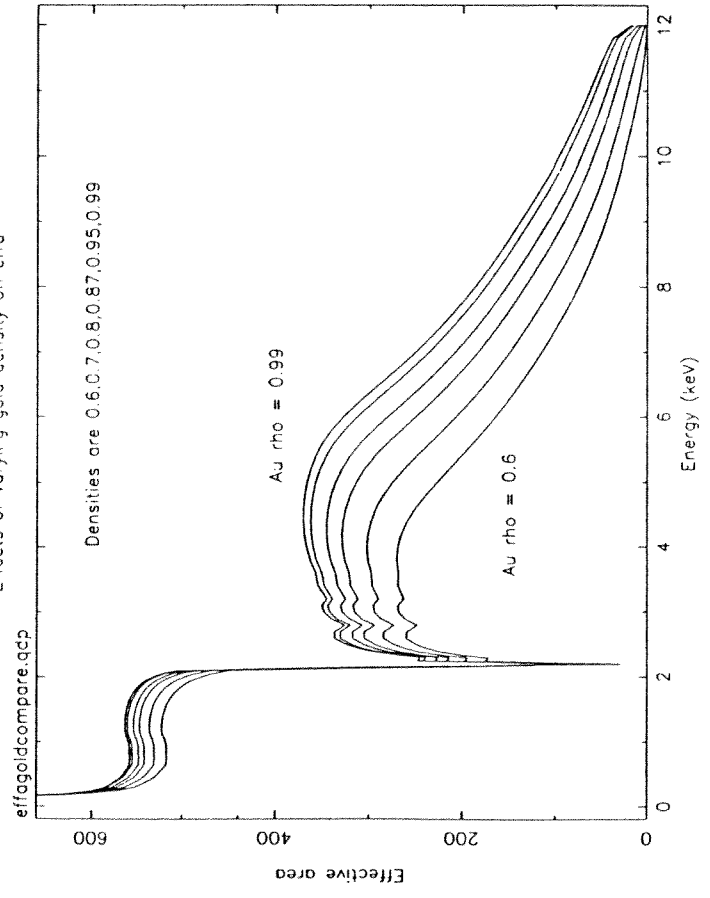
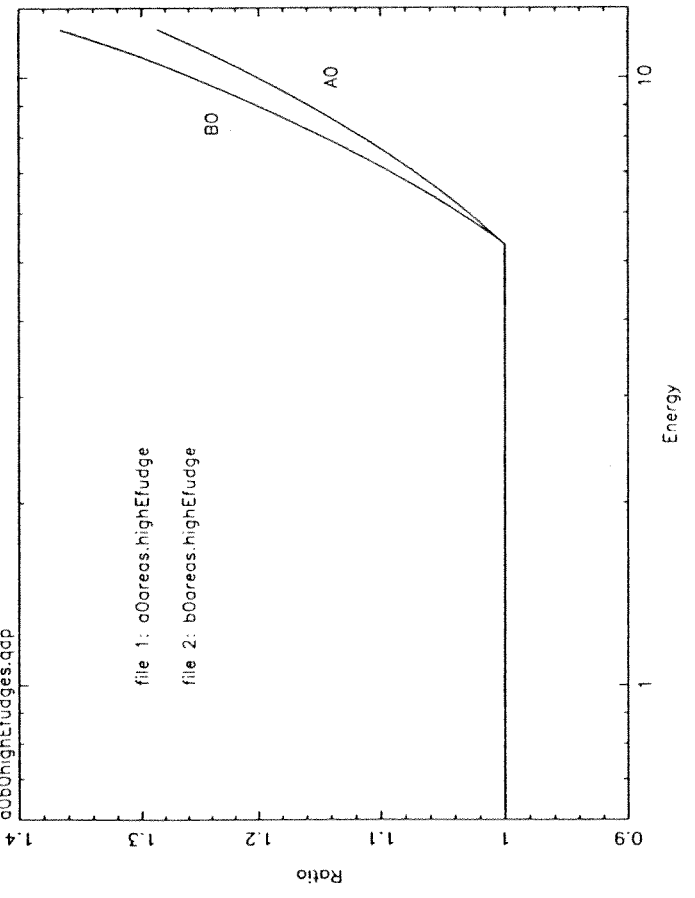


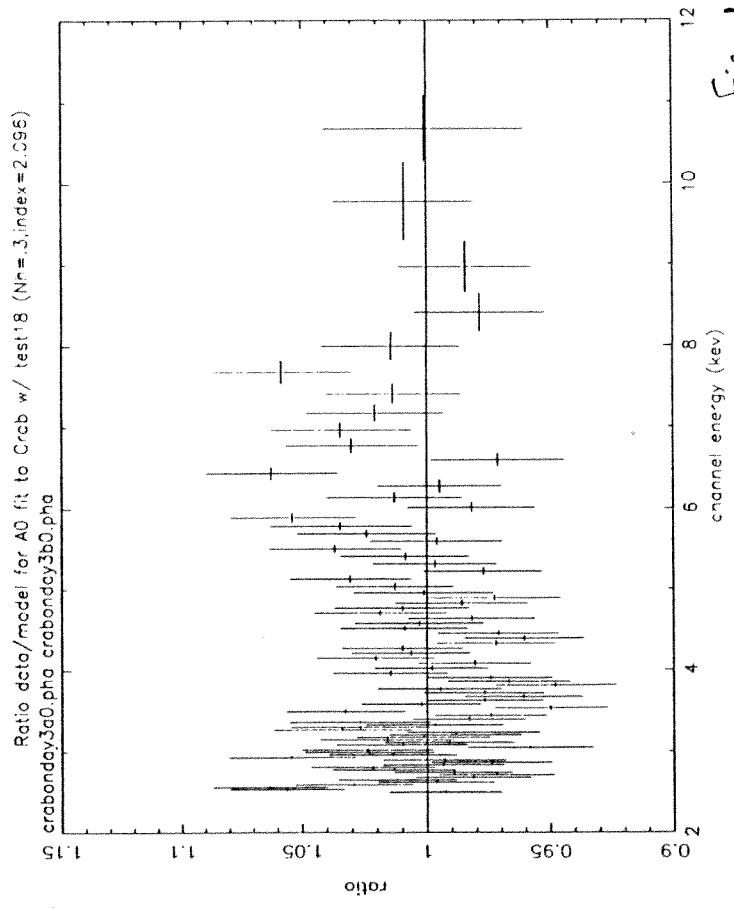
Fig. 9

Multiplicative factor for High Energy effa correction



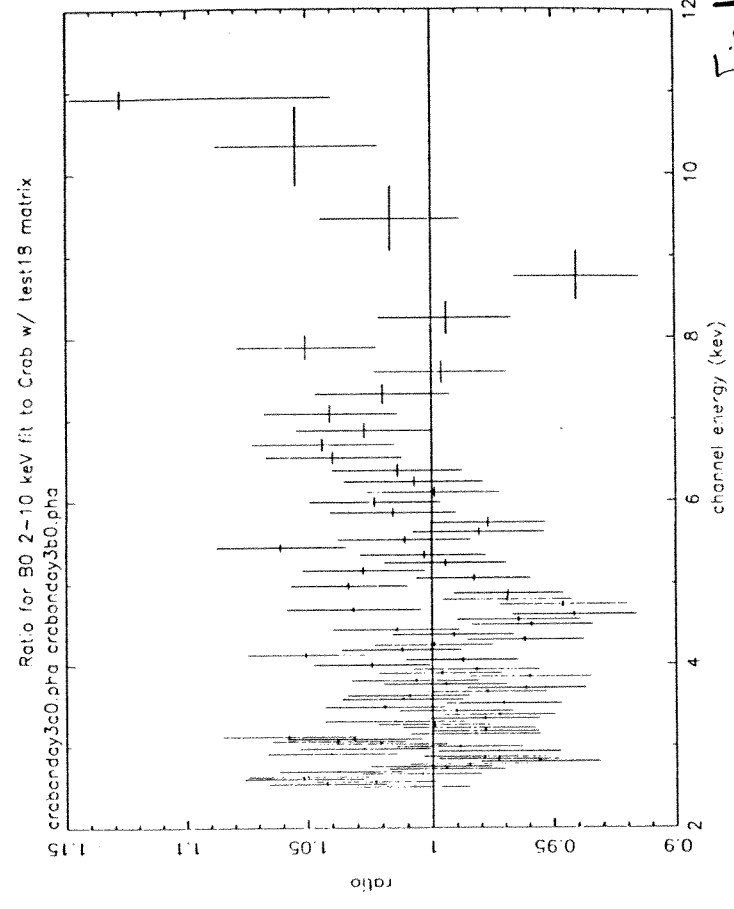
file 1: a0areas.highEfdge
file 2: b0areas.highEfdge

Fig. 10



Ratio data/model for A0 fit to Crab w/ test18 (Nh=3,index=2.096)
crabonday3a0.pha crabonday3b0.pha

Fig. 11a



Ratio for B0 2-10 keV fit to Crab w/ test18 matrix
crabonday3c0.pha crabonday3b0.pha

Fig. 11b

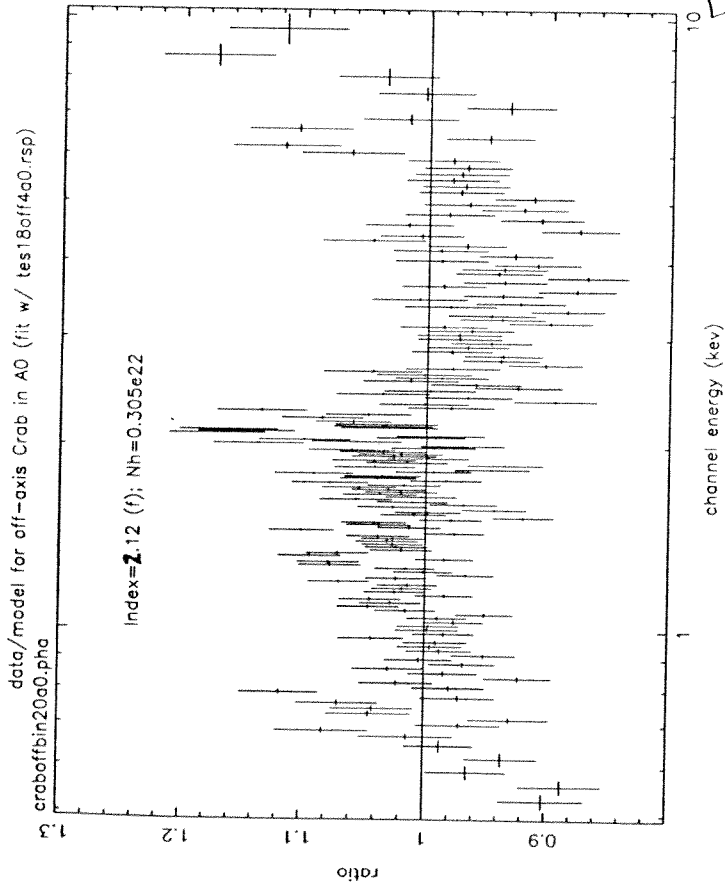


Fig. 12

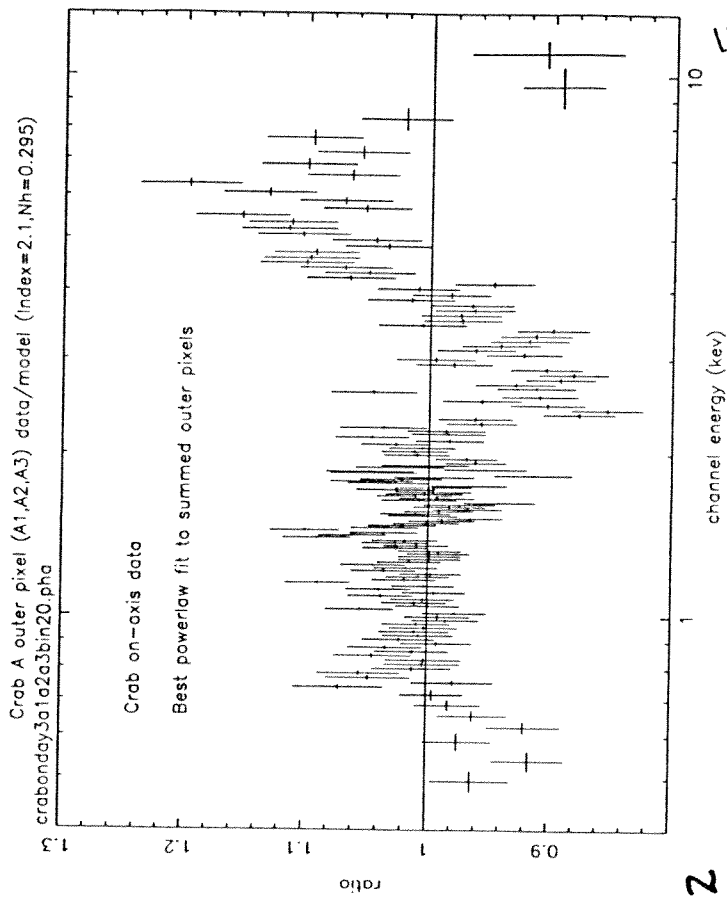


Fig. 13

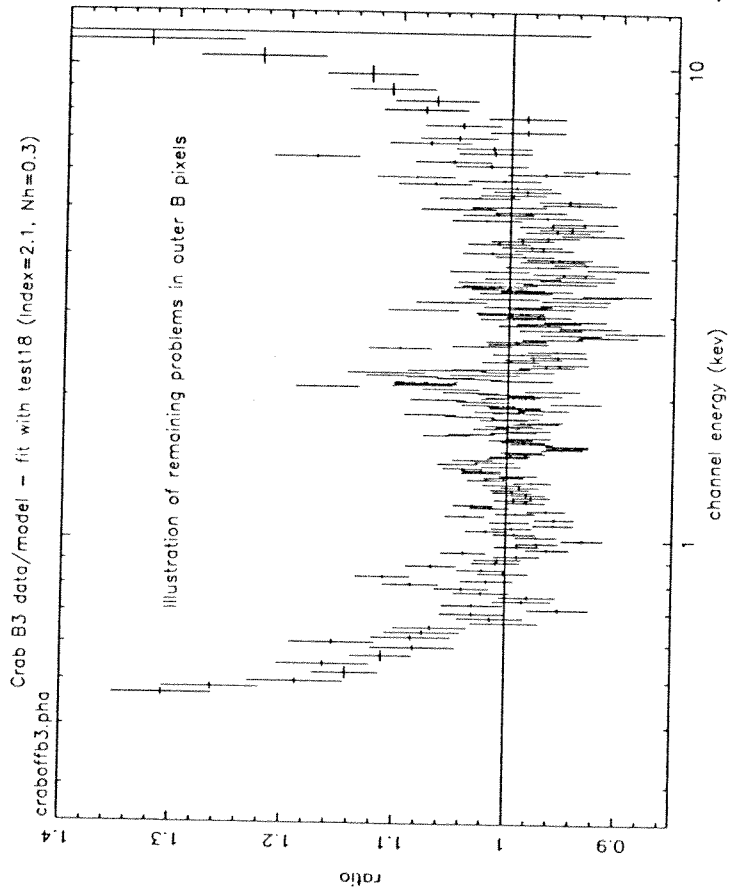


Fig. 14